Simulating and understanding variability in runoff from the Sierra Nevada

UC Water Resources Center Technical Completion Report
Project No. WR1024
January 2010

Principle Investigator:
Alex Hall
Associate Professor
Atmospheric and Oceanic Sciences
University of California, Los Angeles
alexhall@atmos.ucla.edu

Abstract

We have conducted a study of Sierra Nevada runoff by analyzing the onset of snowmelt (or peak snowmass timing) from observations and conducting model simulations of snowpack. For our observation study, monthly snow water equivalent ("SWE") measurements were combined from two data sets to provide sufficient data from 1930 to 2008. The monthly snapshots are used to calculate peak snow mass timing for each snow season. Since 1930, there has been an overall trend towards earlier snow mass peak timing by 0.6 days per decade. The trend towards earlier timing also occurs at nearly all individual stations. Even stations showing an increase in April 1st SWE exhibit the trend toward earlier timing, indicating that enhanced melting is occurring at nearly all stations. Analysis of individual years and stations reveals that warm daily maximum temperatures averaged over March and April are associated with earlier snow mass peak timing for all spatial and temporal scales included in the data set. The influence is particularly pronounced for low accumulation years indicating the potential importance of albedo feedback for the melting of shallow snow. The robustness of the early spring temperature influence on peak timing suggests the trend towards earlier peak timing is attributable to the simultaneous warming trend (0.1ºC per decade since 1930, with an acceleration in warming in later time periods). For our modeling study, we have used the Weather Research and Forecasting Model ("WRF") to model snowpack at high resolution over the Sierra Nevada during the 2001-2002 water year. We have focused on one year to validate the use of WRF for understanding runoff variability. We have found that high resolutions are necessary to accurately model snow cover over the Sierras.

Introduction

The California water supply is determined by cold season precipitation (rain in low elevations and snow in high elevations) and the capacity of natural and man-made reservoirs. Most man-made reservoirs were built in the early 20th century for two purposes: (1) the storage and disbursement of cold season rains and (2) the storage and disbursement of runoff from spring snowmelt. Reservoirs were designed to store only a fraction of the state's total yearly precipitation, under the assumption that a sufficient delay between winter rains and spring snowmelt runoff would always exist, with snowmelt occurring at roughly the same time every year. The annual mountain snowpack thus provides natural storage for the water supply until the onset of snowmelt. Changes in the amount of precipitation, percentage of precipitation falling as rain instead of snow, and onset of snowmelt can therefore affect the state's water supply. During anomalously high rain or snowmelt events, reservoirs must not only store water, but also discharge excess water to avoid flooding. Water must sometimes even be discharged in anticipation of large events to reduce flood risk. The dual functions of storage and flood management require reservoir managers to carefully balance factors such as: precipitation, snowmelt timing, reservoir storage capacity, and demand. Even if future climatological precipitation remains unchanged, shifts in snowmelt timing can affect California's water supply during the warm season due to reservoir storage capacity constraints. To understand changes in snowmelt water supply as a result of climate change, it is therefore

important to understand changes in the timing of snowmelt in addition to total spring snowpack amounts.

Snowpack measurements are essential for predicting timing and amount of warm season snowmelt runoff. For this reason, a network of stations in the Western United States dating back to the 1930s tracks water content of snow (also known as snow water equivalent or "SWE"). Measurements are taken manually around the 1st of the month at each station according to a prescribed monthly schedule. Because of the desire to track peak SWE--thought to occur in early April--many more records are available on or around April 1st (Serreze et al. 1999). Previous snowpack studies have focused on this well-sampled April 1st SWE data set (Barnett et al. 2008, Mote 2006, Mote et al. 2005, Cayan 1996) to assess the climatology and variability of snowpack in the Western United States. These studies are important for understanding total melt water available during the warm months, but do not directly address the timing of the transition from accumulation to melt from snow observations.

Ideally, high-temporal resolution data would be available to study the evolution of the snowpack over the course of the season, particularly the exact date and amount of maximum SWE and subsequent melt rates. Stations have been built in California since the 1970s to measure daily SWE automatically, but do not begin early enough for long-term variability analysis. Previous observational studies have instead utilized streamflow data, presumably snowmelt-dominated, as a proxy for snowmelt timing. They show there has been a trend in streamflow discharge towards earlier in the spring using a variety of streamflow metrics (Regonda et al. 2005, Stewart et al. 2005, Cayan et al. 2001). Daily SWE data from 1992 to 2002 has also been combined with long-term historic streamflow data to study the onset of spring in the Sierra Nevada (Lundquist et al. 2004); however, because of the shortness of the SWE time series, streamflow measurements must still be relied upon to measure long-term variability in snowmelt. Unfortunately, this indirect variable is not a perfect measure of snowmelt, as it can be influenced by other factors such as precipitation, temperature, lithology, soil composition, vegetation (Aguado et al. 1992), and pre-snowmelt soil moisture.

The majority of regional modeling studies of the hydroclimate over the Western United States have been run at a resolution of 36km or coarser (Dickinson et al. 1989; Giorgi et al. 1994; Kim et al. 2002; Leung et al. 2003; Duffy et al. 2006; Kim et al. 2009; Lynn et al. 2009); this resolution is an improvement over coarse resolution global climate model ("GCM") studies, but higher resolutions are still needed to increase the accuracy of snowpack studies over the Sierras. For example, Duffy et al. (2006) found that GCM output at 100km resolution has an absence of snow over the Sierra Nevada. Increasing resolution to 40km using a regional model yields minimal snow over the Sierra Nevada, but still lacks the granularity of the observations and is an order of magnitude smaller.

Objectives

To study changes in the Sierra Nevada snowpack directly and provide a purely empirical background to compare against modeling studies, we first conducted a study focused on observations of monthly SWE. A data set has been compiled from two different sources

to provide sufficient stations with SWE measurements from mid-January through mid-May over a long enough time period to do robust trend and sensitivity analysis. The monthly data is used to infer peak snow mass timing from February to May. We hoped to explain the trend in runoff timing by finding a relationship between peak snowmass timing and other climate variables.

The second part of our study of Sierra Nevada runoff aimed to model a snow season to explore runoff variability. The modeling study was conducted by running a regional climate model, the Weather Research Forecasting Model ("WRF"), over the Sierra Nevada for one snow season. The observation data from the first study has been used to validate the model for future runoff modeling work. In this study we explore what resolution is necessary to capture runoff timing and amount.

Procedure: Observation Study

A snow station data set was compiled from two existing data sets for the state of California: the National Resources Conservation Service ("NRCS") and Water and Climate Center (www.wcc.nrcs.usda.gov/snowcourse/) and the California Department of Water Resources (http://cdec.water.ca.gov/misc/SnowCourses.html). A total of 154 stations across California with recorded SWE data from mid-January to mid-May with at least 30 years of data from 1930 to 2008 are used (see Fig. 1). These stations range in their years of available data. It has been noted that the exact timing of historical monthly snow course measurements can vary, with some measurements being taken within a few days of the 1st-of-the-month measurement date (Cayan 1996). In these measurements, there may also be a systematic shift in the actual date of measurement towards later (Mote et al. 2005). To circumvent these issues we only selected stations with exact measurement dates corresponding to raw SWE data for our analysis. The correlations shown in this paper are noticeably reduced when SWE values are assumed to be 1st-of-the-month values; such employment of SWE measurements may therefore lead to a non-negligible source of random error in the other studies. Subsequent sections will describe criteria used to produce subsets of data for analysis.

Temperature data is also used to diagnose snow accumulation and melt processes. Maximum and minimum daily temperature data from 1930 to 2003 was obtained from the Surface Water Modeling group at the University of Washington from their web site (www.hydro.washington.edu/Lettenmaier/Data/gridded/) the development of which is described by Hamlet and Lettenmaier (2005). This data set was chosen for its long temporal coverage (1915 to 2003) and high spatial resolution (1/8 degree) relative to other pre-satellite era temperature products. This product has also been used in previous snowpack studies (Mote et al. 2005, Hamlet et al. 2005).

To assess inter-annual variations in California snowpack evolution, a metric was developed quantifying systematic changes in snow accumulation and melt timing. In particular, we focused on the timing of peak snow mass. We created a measure of this quantity relying on SWE measurements taken around the 1st-of-the-month from February to May. We used these monthly snapshots rather than daily SWE data because the daily

data are only robustly available from 1980 to the present, too short a time series to calculate long-term trends in maximum SWE timing.

The peak snow mass timing is defined for any given year as the temporal centroid date, also known as the center of mass, of SWE values (SWE centroid date or "SCD") from approximately February 1st to May 1st for stations with complete data over this four month time period. The SCD is given by the equation:

$$SCD = \frac{\sum t_i SWE_i}{\sum SWE_i}$$

Each individual measurement during the season is distinguished by *i*. The SWE measurements are given by *SWE_i* in cm. The value *t_i* is the exact date of the measurement in Julian days and falls within two weeks of the first of the month for February, March, April, and May. The SCD metric is similar to that used in previous studies of streamflow peak timing (Stewart et al. 2005, 2004). Fig. 2a provides a visualization of this calculation for a location and a year when daily data are also available. As is clear from the figure, SCD captures the gross timing of snow processes. For the peak to shift earlier (later), the percentage of snow accumulation later in the season must decrease (increase), or there must be an increase (decrease) in the percentage of snow melting later in the season. Thus it corresponds roughly with the peak in snow mass.

The SCD metric provides a more accurate representation of the timing of snow accumulation and melt than the date of absolute maximum SWE value given in the four approximate 1st-of-the-month point measurements. It allows for the snow mass peak timing to shift on the order of days instead of being constrained to shifts in monthly increments. Long-term variability in snow mass peak timing can be studied on sub-monthly time scales despite the lack of daily data. As we show below, the changes in peak snow mass timing in the Sierra Nevada are order days, confirming the need for a metric with this property.

For stations where daily data are available within close proximity to long-term monthly stations, SCD was calculated on a daily and monthly basis to assess the accuracy of using historical monthly SWE values. Daily SWE values from January 15th to May 15th from 13 stations were used to calculate a "daily SCD", while 1st-of-the-month measurements taken from the daily stations were used to calculate a "monthly SCD". These stations were chosen to correspond to those used in subsequent long-term monthly trend analysis. For each station, years missing 10 or more days from January to May were excluded; this criterion was similarly employed by Knowles et al. (2006) and developed by Huntington et al. (2004). The SCD values calculated from monthly and daily data was found to be extremely highly correlated ($r = 0.98$, $p < 0.01$), giving confidence that the temporal resolution of monthly snapshots is high enough to provide accurate information about snowpack timing.

Procedure: Modeling Study

The Weather Research and Forecasting ("WRF") model version 3.0 was used to study the Sierra Nevada hydroclimate. The following physics options were used: the modified Kain-Fritsch convection parameterization (Kain and Fritsch 2004; Kain 2004), the Thompson et al. (2004) cloud microphysics scheme, the CAM3 shortwave and longwave radiation schemes (Kiehl et al. 1996), and the Yonsei University planetary boundary layer scheme (Hong and Dudhia 2006). More details on the WRF model can be found at the website: http://wrf-model.org.

The hindcast simulation was forced with the North American Regional Reanalysis ("NARR") product (Mesinger et al. 2006). The NARR product covers North America and a portion of the surrounding oceans at 32km resolution with temporal coverage from 1972 to the present. The product was created using the National Center for Environmental Prediction's ("NCEP") Eta model to downscale the NCEP Reanalysis product to 32km, with additional data assimilation to improve the reanalysis product. The NARR product has been proven to be an improvement over the NCEP Reanalysis product with better estimations of pressure, temperature, and precipitation, especially during the winter months (Mesinger et al. 2006). The simulation was run from November 2001 to November 2002.

The model domain has three one-way nested domains at 27km, 9km, and 3km resolution over the Sierras (Figure 7). The outermost domain covers much of the Western United States to capture moisture flow into the region. The 9km domain covers all of California, and the 3km innermost domain covers the Sierra Nevada. The mountain terrain is well represented at this resolution.

Validation of the model output was conducted by comparing daily SWE gridcell values again daily observations from snow stations. While the scale of observations (1 to 10m resolution) is very different than that of model observations (27, 9, or 3km resolution), the observations can give us a rough estimate of when snowmelt should start to occur over the snowpack.

Results: Observation Study

Examination of SCD from 1930 to 2008 yields evidence that it is trending earlier. When stations with data for at least 75% of these years are included, SCD is found to occur earlier at a rate of 0.6 days per decade (Fig. 3; this is similar to figures showing trends in earlier spring timing in Cayan et al. (2001)). This trendline has a slope significantly different than zero (using the Student's T-test, $p < 0.01$). When stations with fewer yearly SCD values are also included, or when the starting year of the trendline is set later to include more stations, statistically significant non-zero trendlines of earlier peak timing are still found (Table 1). In most cases, the trend towards earlier peak timing is enhanced (i.e. the trend becomes more negative). There is a similar enhancement in the averaged March and April maximum daily temperature warming trend from 1930 to 1970 as successively later periods of the time series are isolated (Table 1, last row). We discuss the potential causal link between the warming and SCD trends in the discussion.

Almost all individual station SCD trends are also negative (Fig. 4), suggesting a consistent signal from catchment to catchment. In addition, Fig. 4 compares station trends in SCD to trends in the highly studied April 1st SWE record. (Note that measurements are taken within two weeks of April 1st for the "April 1st SWE record." Mote et al. (2005) noted that the fluctuation in measurement date may affect April 1st SWE trends, but concluded that climatic factors likely have a dominant effect on the trend.) The majority of stations exhibit a negative trend in both SCD and April 1st SWE. A negative SCD trend is associated with snow melting earlier, which also results in trends towards lower SWE. Some of the change in SCD may also be driven by a shift towards more rain and less snowfall as described by Knowles et al. (2006); our analysis shows that only the lowest elevation stations have exhibited statistically significant trends in both metrics.

Fig. 4 resolves the apparent inconsistency between increasing April 1st SWE at some locations and a warming climate. All the points with positive trends in April 1st SWE have negative trends in SCD. These points all have positive trends in SWE from February to May (not shown). Enhanced melting at these locations must therefore be compensating for the increased accumulation to create the negative trend in SCD. The link between April 1st SWE values and melt during previous months has been observed in some daily Snowpack Telemetry ("SNOTEL") stations in the California Sierra Nevada; April 1st SWE was shown to be highly anti-correlated with daily melt events from the previous months, implying changes in April 1st SWE have been due at least in part to melt events (Mote et al. 2005).

Variability in April 1st SWE is evaluated against variability in the SCD metric to explore relationships between SCD and the SWE variable used to predict water supply. Fig. 5 shows a scatterplot of April 1st SWE versus SCD values. Each point represents a snow station during one snow season. Snow stations with a minimum of 75% of SCD values over the period from 1950 to 2003 were used for this analysis. This time period was selected to coincide with the available temperature record and increase the number of snow stations available for temperature sensitivity studies in Section 3d. (A nearly identical distribution is found if the start date is changed to 1930.) For the given subset of snow stations, SCD occurs over a wide range, with the average SCD occurring on Julian day 73 (mid-March). The average April 1st SWE value is 74cm.

The striking bell-shaped distribution of the April 1st SWE versus SCD scatterplot arises because of differing behavior of SCD for large and small seasonal snow accumulation. When April 1st SWE is large (roughly greater than or equal to 100cm), the SCD tends to occur in a narrow band between Julian day 70 and 90, with most points (96%) above the mean of 73. This corresponds to a time period mainly falling between the middle of the 2nd and 3rd bar of Fig. 2, or the calendar month of March. There are three main reasons for this behavior: (1) To attain such high April 1st SWE values, relatively consistent storm activity and steady accumulation is necessary from February to March. (2) The large accumulation then increases the effective thermal inertia of the snowpack, delaying the onset of melting. (3) This large accumulation then only melts once the seasonal warming becomes great enough to initiate the melting process. These three processes make for a late SCD, with little variation from season to season.

When April 1st SWE is small (less than roughly 100cm) however, the SCD falls over a large range between Julian day 21 and 114. This range is more than four times that of the

high seasonal accumulation and covers the middle of the 1st bar to the middle of the 4th bar in Fig. 2, or from the last day in January to the end of April. The significantly greater range in SCD values is due to two factors: (1) Low accumulation is the result of a relatively small number of storms with highly variable timing. (2) Melting in shallow snow is more sensitive to temperatures above freezing because of the smaller thermal inertia of shallow snow and its greater susceptibility to albedo feedback. This results in earlier (later) snowmelt when temperatures are warm (cold).

To explore the sensitivity of SCD to temperature further, the colorbar given in Fig. 5 distinguishes the distribution of SCD values by local averaged March and April ("MA") maximum daily temperature. The local average maximum daily temperature for each station is calculated by taking the local gridcell maximum daily temperature, averaging it over two months, and adjusting it for the elevation of each station assuming a constant lapse rate of 6.5˚C/km. When the distribution of SCD vs. April 1st SWE is distinguished by temperature, SCD has very little systematic association with either January or February temperatures, but is closely linked to early spring temperature (colorbar in Fig. 5). The correlations of observed SCD and temperatures for different months are shown in the first row of Table 2, and clearly quantify the influence of late accumulation-season temperature on SCD. Lower MA temperatures appear to shift SCD into the later half of the season. The most likely reason for this connection is that snowmelt during March and April is reduced (increased) by anomalously cold (warm) March and April temperatures, thus moving SCD to the later (earlier) portion of the season. The sensitivity to MA temperature is particularly pronounced for years when April 1st SWE is low ($r = -0.61$, $p < 0.01$ when April 1st SWE is less than 100cm versus $r = -0.47$, $p < 0.01$ when it is above this threshold), providing direct evidence of the greater susceptibility of shallow snow to fluctuations in temperature and potentially albedo feedback.

Fig. 5 provides visual evidence that air temperature, the primary thermodynamic control of melt, is potentially a major variable affecting SCD. Fig. 6a provides a statistical measure of the link between the MA maximum daily temperature and SCD for the direct observations of these variables. Temperature is found to shift SCD earlier in the season by 2.5 days per degree and is significantly anti-correlated ($r = -0.62$, $p < 0.01$) with SCD. As noted in Section 3b, the trend towards earlier SCD coincides with a trend toward warmer MA temperature. The anti-correlation between SCD and temperature seen in Fig. 6a could result from these two trends. However, when the SCD and temperature time series are detrended, the anti-correlation remains ($r = -0.47$, $p < 0.01$). This suggests the link between MA temperatures and SCD is robust for temporal variability as well as trends in SCD, a point we return to in the discussion.

Figures 6b and 6c reveal the SCD-temperature relationship when controlled for spatial and temporal variability. In Fig. 6b, the temporal SCD and maximum daily temperature anomalies (defined as the observation value minus the mean value at each station) are compared. Here we eliminate any systematic relationship between SCD and temperature in Fig. 6a arising from the fact that the stations are at different locations and therefore have different climatological temperatures. Conversely, in Fig. 6c, temporal variability is eliminated by comparing station mean SCD values against station mean maximum daily temperatures. Thus, each point on the graph is an individual station. A negative relationship between SCD and temperature remains when spatial and temporal variability are each isolated in turn. Moreover, Table 2 shows that MA temperatures have the

greatest overall relationship with SCD from January to May for direct observations, anomalies, and mean station values. This analysis was also conducted using averaged daily minimum temperatures; negative correlations between SCD and temperature remained, but were lower than shown in Fig. 6 and Table 2. This is likely due to maximum temperature being more closely associated with snowmelt given that average minimum temperatures are predominantly below freezing. This analysis provides evidence of the predictive value of MA maximum temperature for both spatial and temporal variability in SCD.

Results: Modeling Study

To quantify the errors associated with using WRF 3.0 to study the hydroclimate of the Sierras, we first compared model simulations with observations. High-resolution nests (on the order of 3km) are necessary to produce SWE values on the same order as observations (Figure 8). However, point observations have shown that the simulated snowpack experiences melt earlier in the season than in reality (Figure 9). This results in lower maximum SWE values and a total loss of snowpack earlier in the season in the simulation. The timing of the onset of snowmelt for the set of snow stations used is correlated with elevation, resulting in low elevation stations experiencing snowmelt before high elevation stations. This is also a hypothesis for why the top two stations in Figure 9 are better correlated with the simulated snowpack than the bottom two stations; stations at lower elevations are experiencing snowmelt significantly earlier than they should and therefore miss accumulation during the time of maximum snowfall. Previous studies have shown that the default values of emissivity and snow albedo in older versions of the Noah land surface model may have been unrealistic and led to a model warm bias leading to the premature onset of snowmelt and abnormally high values of sublimation (Qian et al. 2009; Slater et al. 2007). These values have been changed in the current NOAH land surface model in the most recent WRF model (WRF 3.1.1). We have begun to simulate the snowpack using the new WRF model and have found that snow is not melting as early as it did previously. We are still conducting analysis of our new simulation.

Conclusions

In our observation study, a metric is developed to calculate peak snow mass timing in the California Sierra Nevada using monthly SWE data from 1930 to 2008. Robust statistical analysis is conducted to assess the variability in the timing of peak snow mass. From 1930 to present, the peak timing of the entire data set exhibits a trend towards earlier in the season of 0.6 days per decade. On an individual station basis, most stations show earlier SCD and reduced April 1st SWE, and the only stations with statistically significant trends in both SCD and April 1st SWE exhibit negative trends in both variables. The trends in SCD complicate interpretations of April 1st SWE as a metric of Sierra Nevada snowpack trends as nearly all stations exhibit negative trends in SCD indicating that enhanced melting is occurring even when April 1st SWE may be increasing. The influence of MA temperature on SCD is almost certainly due to the effect

of early spring temperature on snowmelt. This relationship is particularly pronounced for low accumulation years, indicating the lower thermal inertia of shallow snow and potential enhancement of snowmelt due to albedo feedback as bare ground and vegetation is exposed. The robustness in the sensitivity of SCD to MA temperature for all spatial and temporal scales inherent in the data set indicates the SCD trend can be attributed to the MA warming trend.

The trend in snow mass peak timing found in this observation study is less than those of snowmelt-dominated streamflow found in some previous studies (Regonda et al. 2005, Stewart et al. 2005, Cayan et al. 2001), which provide changes in the date of peak runoff on the order of a few days per decade. The differences in the trends in these two metrics may be accounted for by the fact that a shift in the timing of streamflow runoff is not necessarily accompanied by an equal shift in peak snow mass. In fact, if the shift in SCD is due to earlier snowmelt, the snowmelt acceleration would probably have to be much more rapid than the SCD shift. This is due to the steadiness of the weights of the accumulation months (i.e. measurements around February 1st and March 1st) in the SCD calculation. The involvement of four months of data in the SCD calculation introduces more "inertia" into this quantity than snowmelt runoff.

Preliminary analysis of a simulation of the Sierra Nevada hydroclimate has shown that high-resolution grids are necessary to accurately capture SWE variability. The land surface model used in the WRF model greatly affects the timing of snowmelt, and thus runoff. Snowmelt timing in the model appears to be influenced by local temperature, leading to grid cells at higher elevations more accurately capturing snowmelt timing than those at lower elevations. Further analysis must be conducted on hydroclimate simulations using the latest land surface model (in WRF 3.1.1) to better understand runoff variability.

Given the importance of high-resolution snowpack predictions, continued research on the Sierra Nevada snowpack is critical to understanding the state's future water supply. Continuation of SWE measurements is necessary to monitor and predict changes in the water supply from the Sierra Nevada snowpack. Further regional modeling studies of the Sierra Nevada would also be helpful to determine the mechanisms affecting accumulation and melt events and to identify regions where precipitation will shift from being snow-dominated to rain-dominated. Snowmelt runoff will be affected by changes in snowfall amounts and snowmelt timing. An understanding of the mechanisms affecting these variables will help predict the future of the California water supply.

List of Publications

The following two publications have been accepted or published. We foresee that two additional manuscripts on the modeling of snowpack will be produced from this project in the next year.

Kapnick, S. and A. Hall, 2010: Observed climate-snowpack relationships in California and their implications for the future. Accepted to Journal of Climate.

Kapnick, S. and A. Hall, 2009: Observed changes in the Sierra Nevada snowpack: potential causes and concerns. California Environmental Protection Agency and California Energy Commission Report CEC-500-2009-016-F.

References

Aguado, E., D. Cayan, L. Riddle, and M. Roos, 1992: "Climatic fluctuations and the timing of west coast streamflow." J. of Clim., 5, 1468–1483.

Barnett, T., D. Pierce, H. Hidalgo, C. Bonfils, B. Santer, T. Das, G. Bala, A. Wood, T. Nozawa, A. Mirin, D. Cayan, and M. Dettinger, 2008: "Human-induced changes in the hydrology of the western United States." Science Express, 10.1126/science.1152538.

Cayan, D., 1996: "Interannual climate variability and snowpack in the western United States." J. of Clim., 9, 928–948.

Cayan, D., S. Kammerdiener, M. Dettinger, J. Caprio, and D. Peterson, 2001: "Changes in the onset of spring in the western United States." Bulletin of American Meteorological Society, 82, 339–415.

Chen F. and J. Dudhia, 2001: "Coupling an advanced land surface-hydrology model with the Penn State-NCAR MM5 modeling. Part I: Model implementation and sensitivity." Monthly Weather Review, 129(4): 569-585.

Dickinson, R., R. Errico, F. Giorgi, and G. Bates, 1989: "A regional climate model for western United States." Climate Change, 15, 383-422.

Duffy, P., R. Arritt, J. Coquard, W. Gutowski, J. Han, J. Iorio, J. Kim, R. Leung, J. O. Roads, and E. Zeledon. 2006. "Simulations of present and future climates in the Western United States with four nested regional climate models." J. of Clim., 19, 873–895.

Giorgi, F., C. S. Brodeur, and G. T. Bates. 1994: "Regional climate change scenarios over the United States produced with a nested regional climate model." J. of Clim., 7,375–399.

Hamle, A., and D. Lettenmaier, 2005: "Production of Temporally Consistent Gridded Precipitation and Temperature Fields for the Continental United States." J. of Hydrometeo., 6, 330-336.

Hamlet, A., P. Mote, M. Clark, and D. Lettenmaier, 2005: "Effects of temperature and precipitation variability on snowpack trends in the western United States." J. of Clim., 18, 4545–4560.

Hong S-Y, Y. Noh, and J. Dudhia, 2006: "A new vertical diffusion package with an explicit treatment of entrainment processes." Monthly Weather Review 134(9): 2318 – 2341.

Huntington, T., G. Hodgkins, B. Keim, and R. Dudley, 2004: "Changes in the proportion of precipitation occurring as snow in New England (1949-2000)." J. of Clim., 17, 2626–2636.

Kain J., 2004: "The Kain – Fritsch convective parameterization: An update." Journal of Applied Meteorology, 43, 170 – 181.

Kain J., and J. Fritsch, 2004: "Convective parameterization for mesoscale models: The Kain-Fritsch scheme." The Representation of Cumulus Convection in Numerical Models, Meteorological Monographs, No. 24, American Meteorological Society, 165-170.

Kiehl J., J. Hack, G. Bonan B. Boville, B. Briegleb, D. Williamson, and P. Rasch, 1996: "Description of the NCAR Community Climate Model (CCM3)." NCAR Tech. Note, NCAR/TN-4201STR, 152.

Kim, J., Fovell, R., Hall, A., Li, Q., Liou, K., McWilliams, J., Xue, Y., Qu, X., Kapnick, S., Waliser, D., Eldering, A., Chao, Y., and R. Friedl, 2009: "A projection of the cold season hydroclimate in California in mid-21st century under the SRES-A1B emission scenario." California Environmental Protection Agency and California Energy Commission Report CEC-500-2009-029-F.

Kim, J., T. Kim, R. W. Arritt, and N. Miller, 2002: "Impacts of increased atmospheric CO2 on the hydroclimate of the Western United States." J. of Clim., 15, 1926–1942.

Kim, J., and J. Lee. 2003: "A multiyear regional climate hindcast for the western United States using the Mesoscale Atmospheric Simulation model." J. of Hydromet., 4, 878–890.

Knowles, N., M. Dettinger, and D. Cayan, 2006: Trends in snowfall versus rainfall in the western United States. J. of Clim., 19, 4545–4559.

Leung, R., Y. Qian, X. Bian, W. Washington, J. Han, and J. O. Roads. 2004: "Mid-century ensemble regional climate change scenarios for the Western United States." Climatic Change, 6, 75–113.

Lundquist, J., D. Cayan, and M. Dettinger, 2004: "Spring onset in the Sierra Nevada: When is snowmelt independent of elevation?" J. of Hydromet., 5, 327–342.

Lynn, B., R. Healy, and L. Druyan, 2009: "Quantifying the sensitivity of simulated climate change to model configuration." Climatic Change, 92, 275-298.

Mesinger, F., G. DiMego, E. Kalnay, K. Mitchell, P. Shafran, W. Ebisuzaki, D. Jovi, J. Woolen, E. Rogers, E. Berbery, M. Ek, Y. Fan, R. Grumbine, W. Higgins, H. Li, Y. Lin, G. Manikin, D. Parrish, and W. Shi, 2006: "North American Regional Reanalyasis." Bull. Amer. Meteor. Soc., 87(3), 343-360.

Mote, P., 2006: "Climate-driven variability and trends in mountain snowpack in western North America." J. of Clim., 19, 6209–6220.

Mote, P., A. Hamlet, M. Clark, and D. Lettenmaier, 2005: "Declining mountain snowpack in western North America." Bulletin of American Meteorological Society, 86, 39–49.

Qian, Y., Ghan, S., and L.R. Leung, 2009: "Downscaling hydroclimatic changes over the Western US based on CAM subgrid scheme and WRF regional climate simulations." International Journal of Climatology. DOI: 10.1002/joc.1928.

Regonda, S., B. Jagopalan, M. Clark, and J. Pitlick, 2005: "Seasonal cycle shifts in hydroclimatology over the western United States." J. of Clim., 18, 372–384.

Serreze, M., M. Clark, R. Armstrong, D. McGinnis, and R. Pulwarty, 1999: "Characteristics of the western united states snowpack from snowpack telemetry (snotel) data." Water Resources Research, 35, 2145–2160.

Slater, A., T. Bohn, J. McCreight, M. Serreze, and D. Lettenmaier, 2007: "A multimodel simulation of pan-Arctic hydrology." J. of Geophys. Res. Biogeo., 112, G04S45, doi:10.1029/2006JG000303.

Stewart, I., D. Cayan, and M. Dettinger, 2004: "Changes in snowmelt runoff timing in western North America under a 'business as usual' climate change scenario." Climatic Change, 62, 217–232.

Stewart, I., D. Cayan, and M. Dettinger, 2005: "Changes toward earlier streamflow timing across western North America. J. of Clim.." 18, 1136–1155.

Thompson, G., R. M. Rasmussen, and K. Manning, 2004: "Explicit forecasts of winter precipitation using an improved bulk microphysics scheme. Part I: Description and sensitivity analysis." Mon. Wea. Rev., 132, 519–542

Tables

Table 1: Trend in peak timing (days per decade) for collective stations and temperature (degrees per decade) found in the gridcells covering the snow stations from start date (denoted in columns) to 2008. Trend in peak timing is given for three different cases: all stations with available SCD data, stations with data for only 50% of available years, and stations with data for only 75% of available years. The bolded cell gives the SCD trend corresponding to Fig. 3. Trend in average monthly maximum daily temperature at elevations above 1700m (elevation minimum for snow stations used in the bulk of this analysis) is given from start date to 2003 (due to the limitation of the available

temperature data set) for the months of January, February, March, and April with the last row providing the averaged March and April temperature trend.

Case	1930	1940	1950	1960	1970
All Stations	-0.7	-0.8	-0.7	-0.7	-0.4
50% of Yrs	-1.0	-1.1	-0.7	-0.7	-0.7
75% of Yrs	**-0.6**	-0.9	-0.8	-1.0	-0.5
January Temp	0.3	0.3	0.5	0.5	0.7
February Temp	0.2	0.2	0.1	0.0	-0.1
March Temp	0.2	0.3	0.4	0.5	0.7
April Temp	0.0	0.1	0.1	0.3	0.5
May Temp	0.1	0.2	0.3	0.3	0.2
Averaged March & April Temp	0.1	0.2	0.3	0.4	0.6

Table 2: Correlation of temperature versus SCD for 70 stations from 1950 to 2003 for January through May and for direct observations, anomalies, and mean values of these variables. This table provides a sensitivity analysis of the correlations found in Fig. 6 (the last column, bolded) for different months.

Sensitivity	January	February	March	April	May	**Averaged March & April**
Direct Observation	-0.21	-0.21	-0.56	-0.52	-0.28	**-0.62**
Anomaly	0.04	0.02	-0.52	-0.49	-0.10	**-0.65**
Station Mean	-0.55	-0.60	-0.65	-0.60	-0.60	**-0.63**

Figures

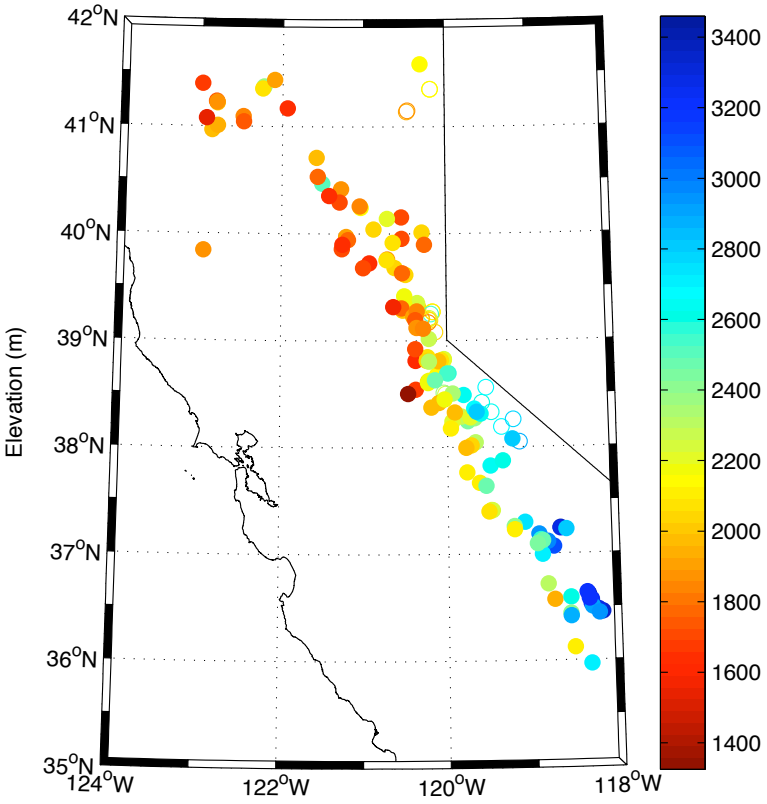

Figure 1: Location of 154 snow stations with usable data in the California. Open circles denote NRCS Water and Climate Center stations and closed circles denote California Department of Water Resources stations. Stations are colored by elevation in meters.

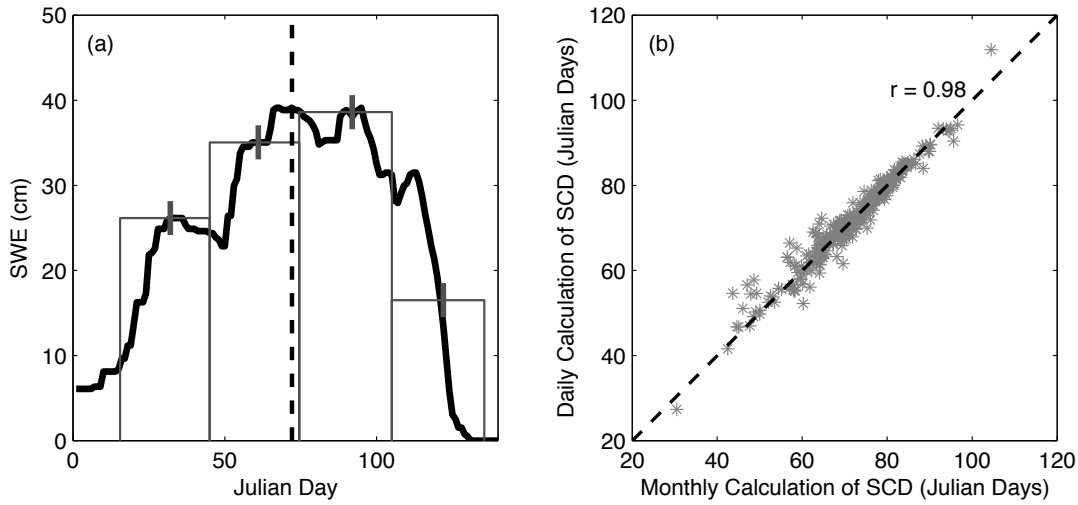

Figure 2: SCD monthly calculation example for one station in 1996 (a) and a comparison of the monthly vs. daily calculations of SCD for 13 stations (b). In (a), the solid black line

denotes daily 1996 SWE values at the SNOTEL Adin Mtn station from January 1st to May 31st. The grey bars help illustrate how four measurements of SWE values are used to calculate the SCD over the time period shown. The grey hatch on each bar denotes the first of February, March, April, and May. The black dashed line at Julian Day 72 denotes the SCD found by using the monthly SCD values. In (b), 13 stations with daily data were used to calculate SCD using the daily and monthly methods. The stations were chosen by their proximity to stations used in the long trend analysis shown in Fig. 3. The monthly approximation of SCD is well correlated with the daily calculation of SCD ($r = 0.98$, $p < 0.01$). There are 336 data points for 13 stations from 1970 to 2008.

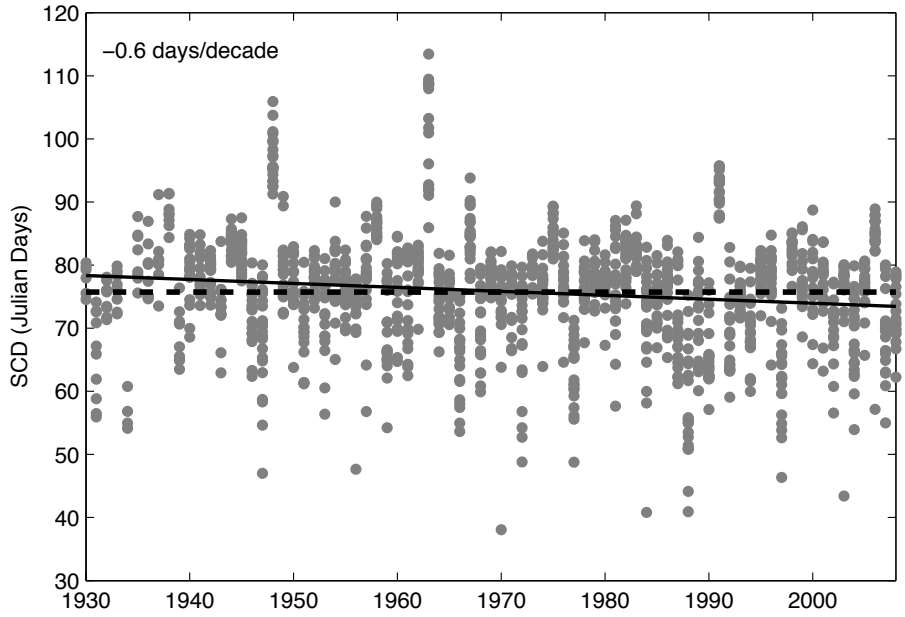

Figure 3: SCD for 22 stations with annual data available for at least 75% of the record from 1930 to 2008. There are 1,482 data points for the time period. The dashed line denotes the mean SCD (Julian day 76) and the solid line denotes the linear trendline for the time series.

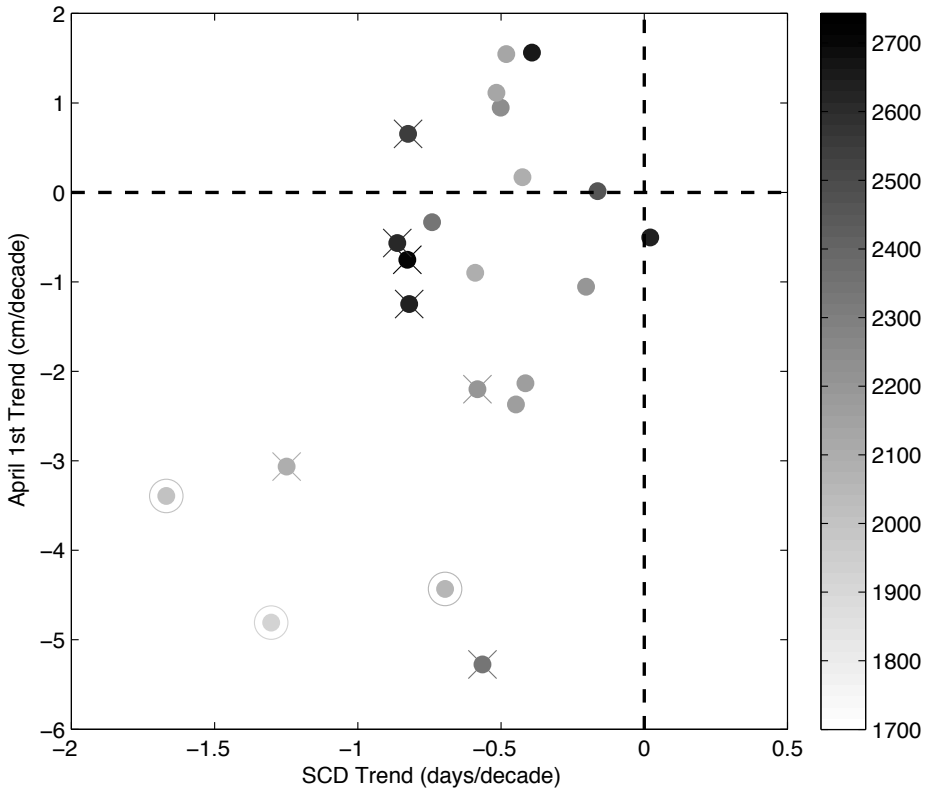

Figure 4: Trend in SCD versus trend in April 1st SWE for 22 stations with at least 75% of years available from 1930 to 2008. Stations are the same ones used for Fig. 3. Dashed lines denote trends of zero. Stations are colored by elevation in meters. Circled stations have statistically significant trends (at $p < 0.05$) in April 1st SWE and SCD. Stations with an x have statistically significant trends (at $p < 0.05$) in April 1st SWE or SCD.

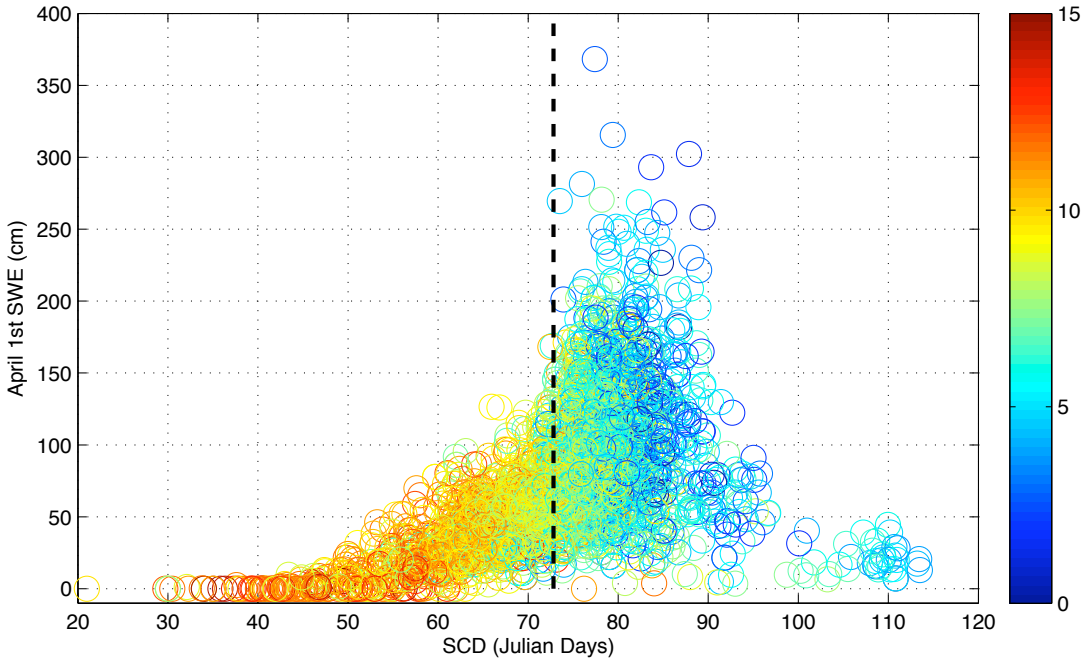

Figure 5: Scatterplot of SCD versus April 1st SWE value for 70 stations with at least 75% of years available from 1950 to 2003; colored by the local averaged March and April daily maximum temperature. Temperature data is from the Hamlet and Lettenmaier (2005) data set (available from 1915 to 2003) and has been adjusted for station elevation assuming a constant lapse rate of 6.5˚C/km. If the graph is confined to stations with at least 75% of years available from 1930 to 2003, a similar distribution is found. The average SCD for the data set is Julian day 73, and is given by the dashed black line.

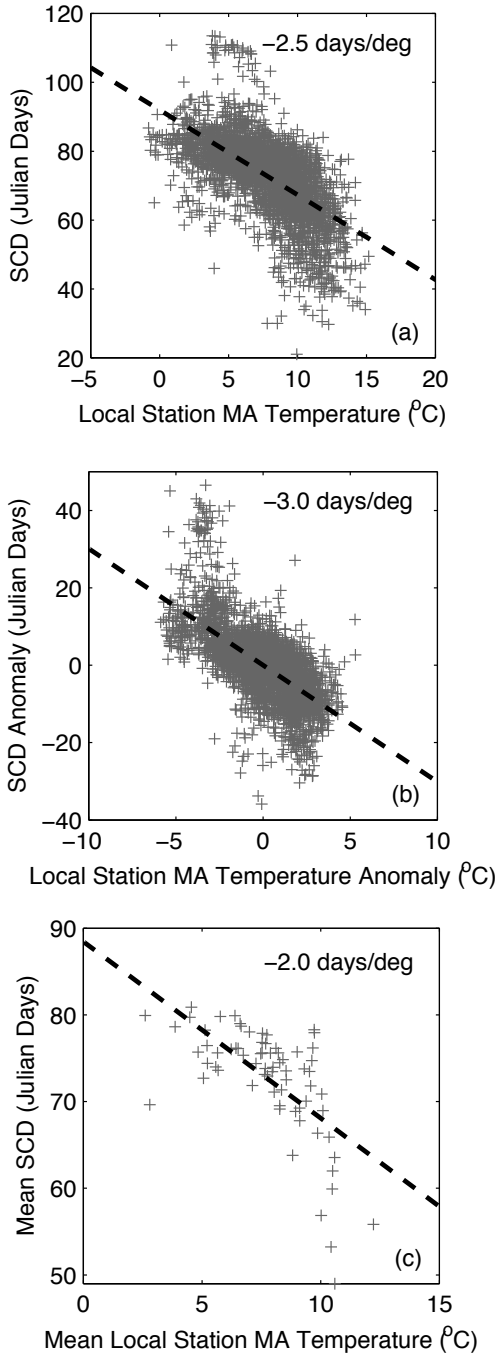

Figure 6: Scatterplot of averaged March and April daily maximum temperature versus SCD for 70 stations from 1950 to 2003 for: (a) observations of SCD and local temperature, (b) anomalies, and (c) mean values. The dashed black line denotes the linear trendline on each graph. The two variables are strongly anti-correlated for all plots: (a) r = -0.62, (b) r = -0.65, and (c) r = -0.63, with $p < 0.01$ for all graphs. If the correlation is calculated for the detrended direct observations and detrended anomalies, the anti-correlations are slightly lower(r= -0.47 in each case), but still material.

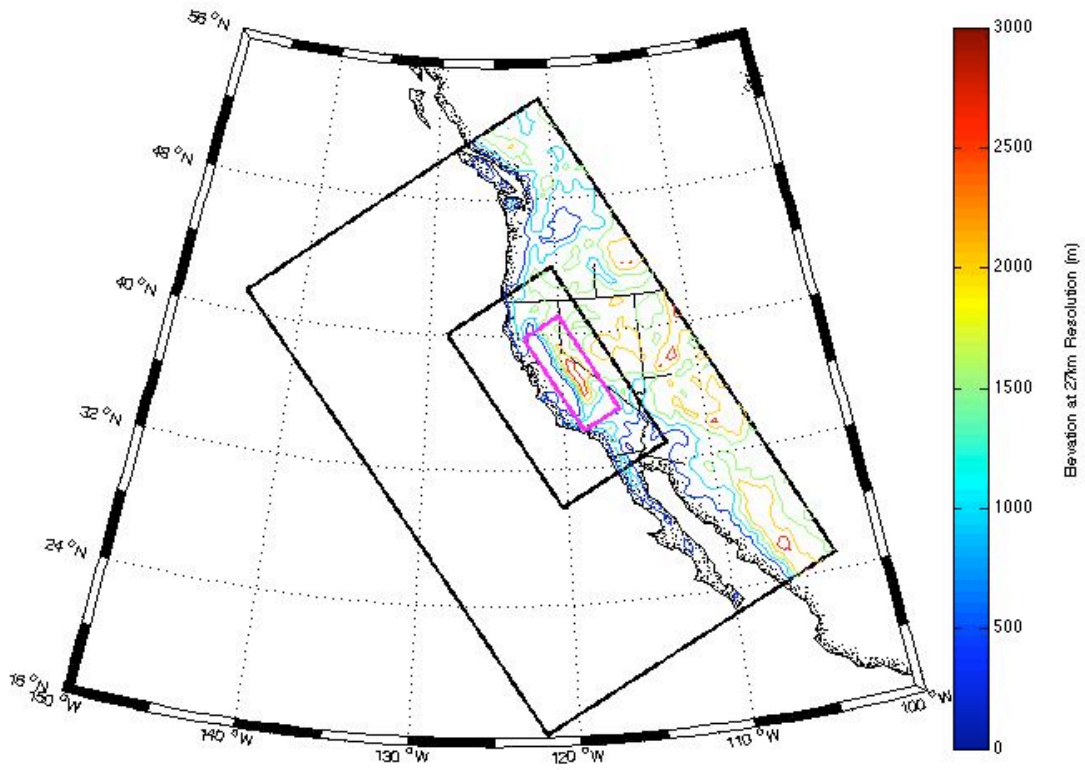

Figure 7: Three domains of the WRF 3.1 simulation. The horizontal resolutions from the outermost to the innermost domain are: 27km, 9km, and 3km (in magenta).

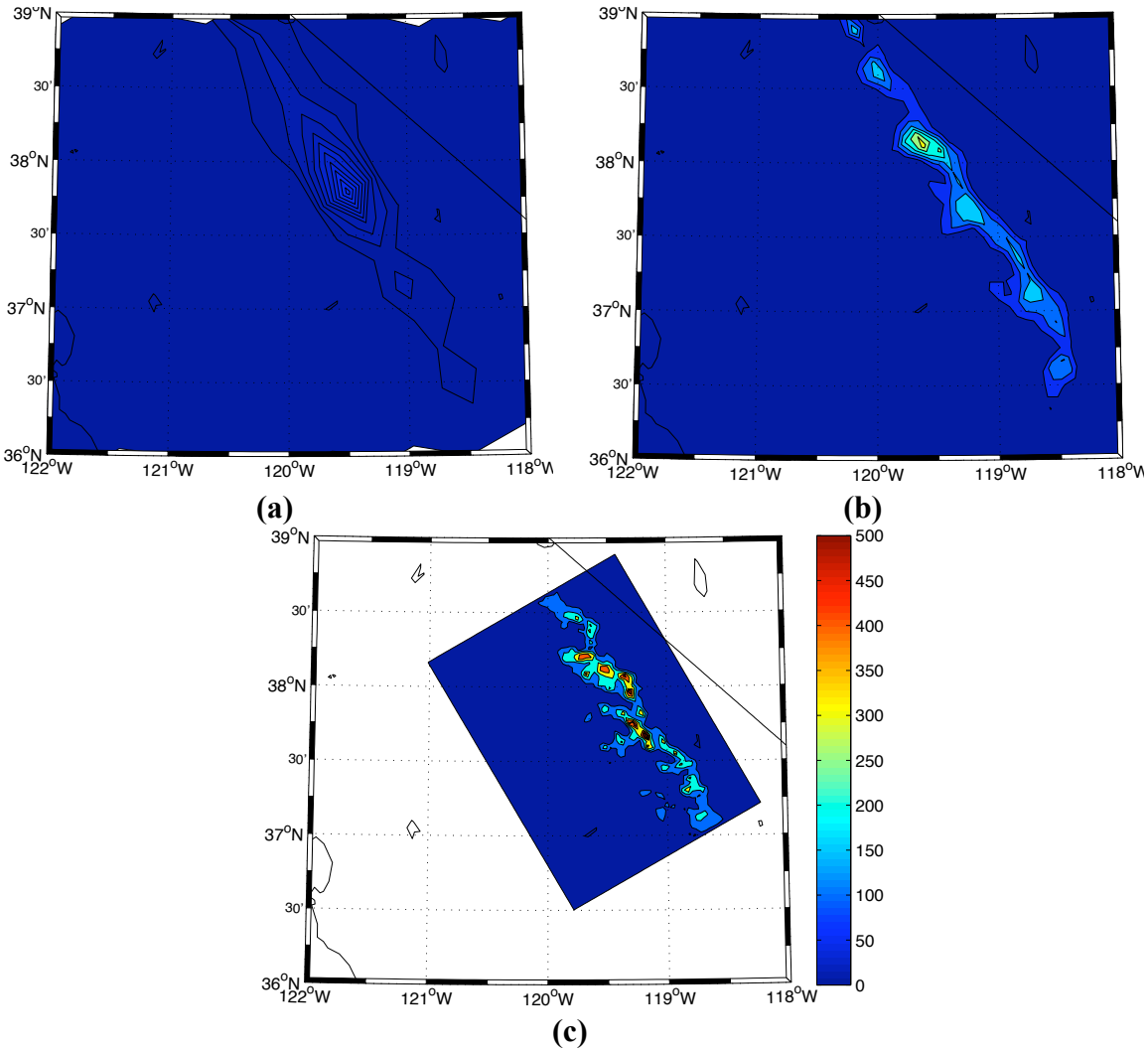

Figure 8: SWE averaged for WRF 3.0 forced by NARR for 2002 MAM at resolutions of (a) 27km, (b) 9km, and (c), 3km. SWE values given in mm.

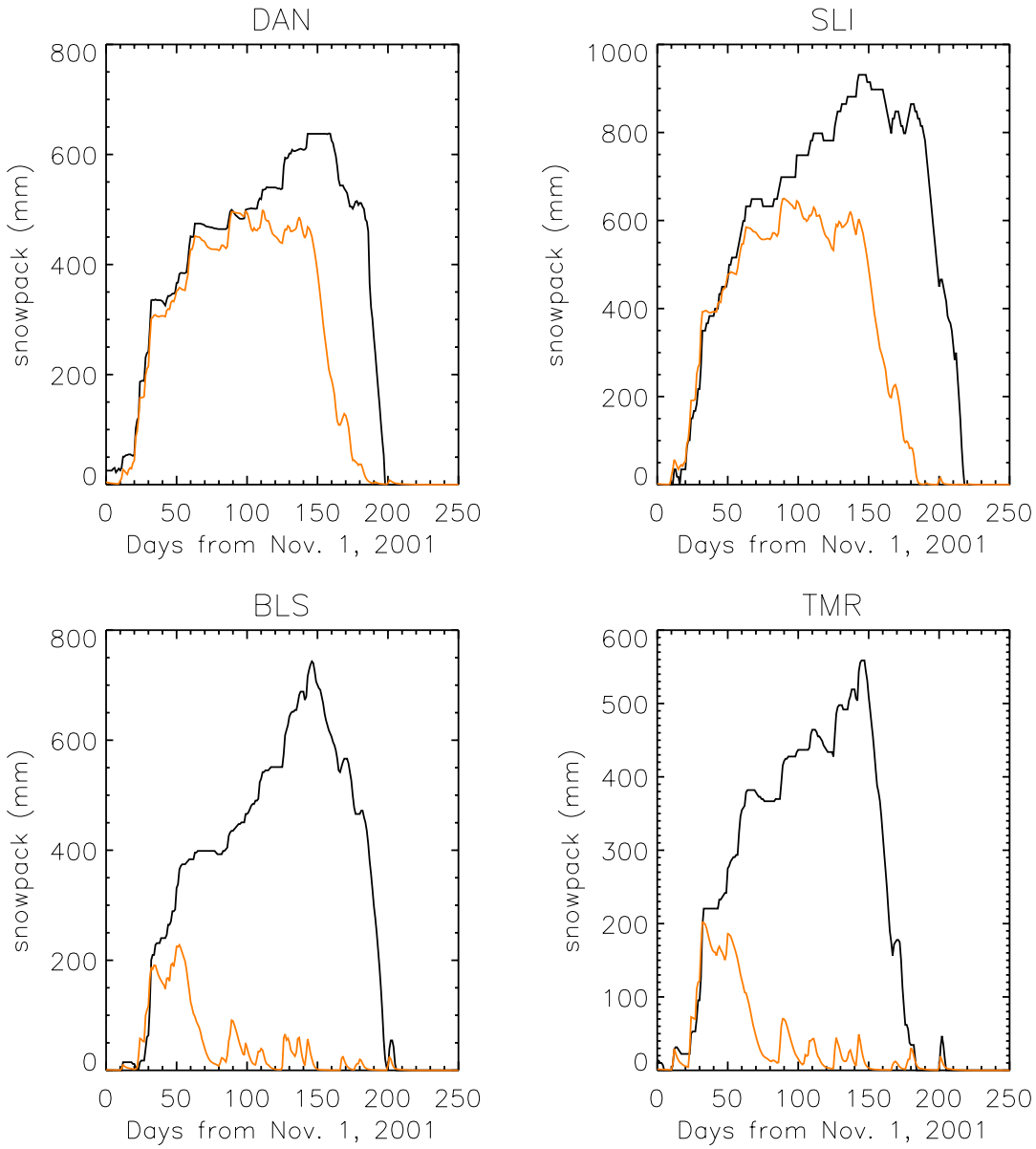

Figure 9: Comparison of modeled WRF 3.0 SWE (orange) at 3km resolution versus observed SWE (black) from snow stations in the Sierras. Two of the best-simulated stations are shown in the top row and two of the worst-simulated stations are shown in the bottom row. Note that all observations when compared to simulated snowpack values showed melt occurring later, suggesting that there is a problem with the land surface model. These four stations are shown in the map of Figure 10.

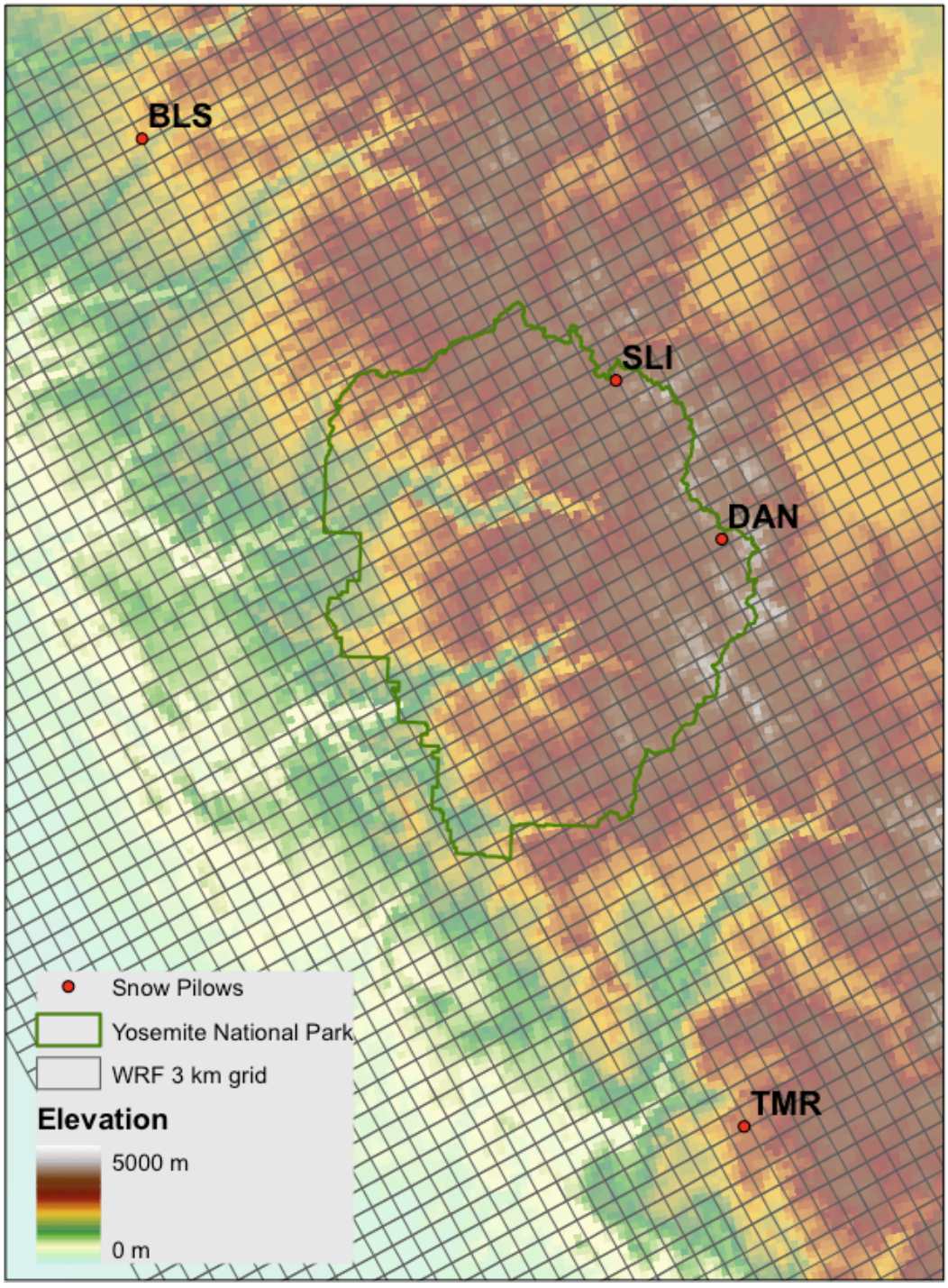

Figure 10: Map of WRF 3.0 3km domain (hatched area) centered over Yosemite National park (green outline). 4 sample snow pillow stations given in Figure 9 shown as red dots.